25th ABCM International Congress of Mechanical Engineering
October 20-25, 2019, Uberlândia, MG, Brazil

COB-2019-0466
PERFORMANCE A SSESSMENT OF AN ELECTRIC REMOTELY PILOTED AIRCRAFT EMPLOYING RIGID BODY MODEL

Vinícius Santos Pereira
Pedro Paglione
Federal University of Santa Maria 1000 Roraima Ave, Santa Maria
vinicius.bezinho@gmail.com
pedro.paglione@gmail.com

André Luís da Silva
Federal University of Santa Maria 1000 Roraima Ave, Santa Maria
andre.silva@ufsm.br

The use of remotely piloted aircrafts (RPA) in the most miscellaneous applications is in continuous growing in the global market, with Brazil being one of the most advanced countries in legislation for regulation of such uses. Having this scenario in mind, the current study was developed in association with Auster Tecnologia enterprise, which develops RPA, to make the performance assessment of an AT190, a fixed-wing, aft-tail and tractor propulsion aircraft produced by the company. This was accomplished theoretically by mathematical modeling and numerical simulation aided by MATLAB & Simulink, employing the classical rigid body equations altogether with simplified electrical modeling of the propulsive system; this being consisted by a double blade propeller, a single brushless motor, electronic speed controller (ESC) and lithium polymer battery (LiPo). The results are going to be incorporated to the user's manual to be provided with the airplane; for this reason, special attention has been given to range and endurance data, in a way that facilitates mission planning.

Keywords: *RPA, Performance, Rigid body, Numerical simulation, Electric motor.*

1. INTRODUCTION

The major objectives of this paper are to assess the airplane performance via numerical simulation of a rigid body aided by MATLAB & Simulink and implement automatic control for trimming the aircraft. This way would be possible to get a close approximation of the range and endurance of the system without having to run a simulation every time a new mission had to be executed.

The specific objectives are:

- Model the remotely piloted aircraft (RPA) mechanics as a rigid body as well as the electro-mechanics of the propulsive system and the aerodynamics of the RPA;
- Design control systems;
- Assess the performance of the vehicle in cruise flight, climb, glide and coordinate turns;
- Estimate the operational radius of the system;
- Draw the flight envelopes in straight flight and in turns.

2. MATHEMATICAL MODEL

All the airplanes systems and subsystems were modeled theoretically applying aircraft design techniques, rigid body dynamics and electro-mechanical modeling.

2.1. Axis Systems

Stevens, Lewis and Johnson (2016) state that a Flat-Earth model is reasonable choice when the distances traveled are within a few hundred miles, then they employ four different axis systems in the study of a rigid body in tridimensional space, one fixed to the Earth and three fixed to the body of the airplane. The Earth or Fixed axis system $X_0Y_0Z_0$ has the plane Y_0Z_0 tangent to the Earth in its origin at sea level and X_0 pointing north, Y_0 pointing east and Z_0 downward.

The first of the three body fixed frames is the Body frame $X_bY_bZ_b$ itself, its origin is in the airplane center of gravity (CG), X_b belongs to the plane of symmetry and points toward the nose parallel to fuselage horizontal plane, Y_b is perpendicular pointing to the right half wing and Z_b completes the right-hand system.

Rotated α around Y_b is the stability axis system $X_sY_sZ_s$ (where the aerodynamic coefficients will be written), making another rotation of β around Z_s there is the wind axis system $X_wY_wZ_w$ which has the X-axis pointed in to the opposite direction of the relative wind. The former announced angles α and β are, respectively, the angle of attack (AOA) and the angle of sideslip. The body-fixed frames can be seen in Fig. 1.

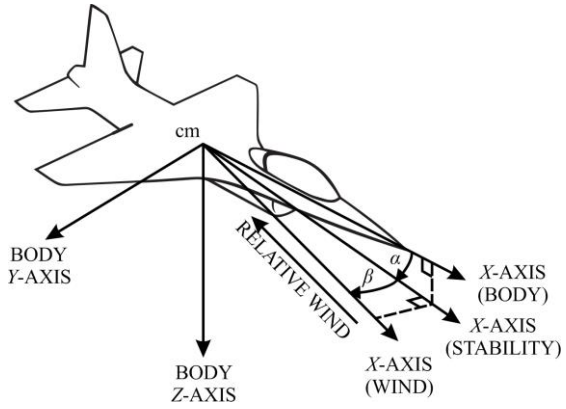

Figure 1. Body-fixed airframes.
Available from: (STEVENS; LEWIS; JOHNSON, 2016).

The aircraft attitude relative to the fixed-frame can be expressed by three Euler angles around the body axis in the order Z-Y-X.

2.2. Movement variables

As proposed by Cook (2007, p. 14) the variables taken in account to develop this work are exposed in Table 1:

Table 1. Description of the movement variables.

F_X F_Y F_Z	Axial force Lateral force Normal force	Force components due to aerodynamics, traction and weight
u v w	Axial velocity Lateral velocity Normal velocity	Linear velocity components
X_0 Y_0 Z_0	North position East position Vertical position (opposite of altitude H)	Position vector components in the Earth-fixed system
ℓ m n	Rolling moment Pitch moment Yaw moment	Moment components due to aerodynamics, traction and weight
p q r	Rolling velocity Pitch velocity Yaw velocity	Angular velocity components
ϕ θ ψ	Roll attitude Pitch attitude Yaw attitude	Euler angles of the body system relative to Earth-fixed system.

Available from: Cook (2007).

According to Steven, Lewis and Johnson (2016), although the linear velocity in the previous table is written in the body system, there are advantages to work in the wind system, this way the velocity in the body frame will be written as follows:

$$\begin{bmatrix} u \\ v \\ w \end{bmatrix} = \begin{bmatrix} V\cos(\alpha)\cos(\beta) \\ V\sin(\beta) \\ V\sin(\alpha)\cos(\beta) \end{bmatrix} \tag{1}$$

2.3. Controls

The airplane has the four standard control devices: rudder, elevator, ailerons and throttle.
- Ruder can deflect 30 degrees for each side and is represented by the symbol δ_r;
- Elevator can deflect 25 degrees up and 20 down and is represented by δ_e.;
- Ailerons can deflect 20 degrees for each side and are represented by δ_a;
- Throttle varies from zero to one and is represented by the symbol π.

2.4. Aerodynamic forces and moments

The aerodynamics forces and momentums are the ones defined by Roskam (1971, 1987, 2001) and so are represented by the following set of equations as the author presented:

$$D_s = C_{Ds} \cdot \bar{q} \cdot S \tag{2}$$

$$L_s = C_{Ls} \cdot \bar{q} \cdot S \tag{3}$$

$$m_s = C_{ms} \cdot \bar{q} \cdot S \cdot \bar{c} \tag{4}$$

$$\ell_s = C_{\ell s} \cdot \bar{q} \cdot S \cdot b \tag{5}$$

$$F_{Ys} = C_{Ys} \cdot \bar{q} \cdot S \tag{6}$$

$$n_s = C_{ns} \cdot \bar{q} \cdot S \cdot b \tag{7}$$

Where D_s, L_s, m_s, ℓ_s, F_{Ys} and n_s are drag force, lift force, pitch moment, rolling moment, lateral force and yawing moment. Their nondimensional coefficients and represented by C_{Ds}, C_{Ls}, C_{ms}, C_{ls}, C_{FYs} and C_{ns}; $\bar{q}$ is the dynamic pressure over the aircraft, S is the reference area, b the wingspan and c is the mean aerodynamic chord (MAC).

2.5. Propulsive system

As shown in the diagram of Fig. 2, a LiPo battery pack, an electronic speed controller (ESC) and a brushless DC motor compose the propulsive system, which powers a two bladed propeller.

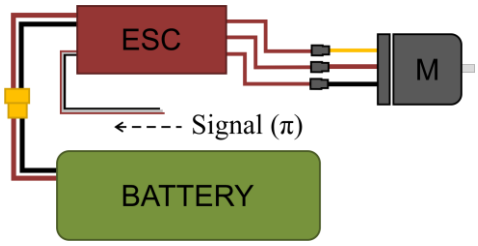

Figure 2. Electric diagram of the propulsive system.
Source: Author.

The model of the battery is the one proposed by Maoquan and Haixin (2017); it is made of a voltage source E_{bat} (V) in series with an internal resistance R_{bat} (Ω) as shown in Fig. 3. The voltage source varies accordingly to current consumption Q (As) and is defined by

$$E_{bat} = E_0 - K_{bat}\frac{Q_0}{Q_0 - Q} + A_{bat} \cdot e^{-B_{bat} \cdot Q} \text{ where } Q = \int Idt \tag{8}$$

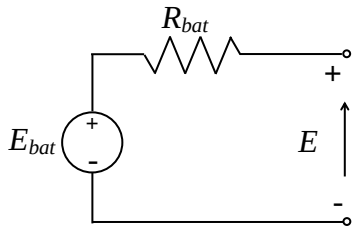

Figure 3. Battery model.
Source: Adapted from Maoquan and Haixin (2017).

The variables E_0 and Q_0 are the battery constant voltage (V) and battery capacity (As), A_{bat}, B_{bat} and K_{bat} are constant parameters estimated by the discharge curve.

The motor is also modeled as proposed by Maoquan and Haixin (2017); the circuit can be seen in Fig. 4, where E_{in} and I_{in} are the input voltage and current. The power losses of the system are represented by an internal resistance R_m (Ω) and the no-load current I_0 (A/V), the resultant voltage E_m and current I_m are converted integrally into mechanical power.

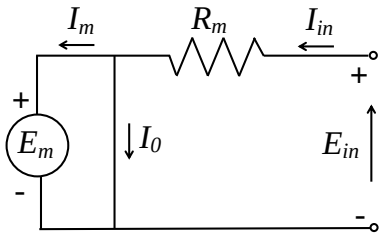

Figure 4. Motor model.
Available from: Maoquan and Haixin (2017).

The influence of the ESC was neglected, considering just a linear relation between power and throttle signal.

At last, the manufacturer provided performance data of the propeller and hence a polynomial function was estimated to fit properly the data given. The result is a function that returns the amount of thrust generated F (N) due to a specific aerodynamic speed V_a (m/s), air density ρ (kg/m³) and input power P_E (W) as follows:

$$F_0 = f(P_E, V), \text{ where } F = F_0 \cdot \rho / \rho_0 \tag{9}$$

2.6. Rigid body model

All the simulations were done applying a methodology proposed by Steven, Lewis and Johnson (2016) for nonlinear models, in which a function f gives the state derivatives for a specific state X and control U and the output is given by a function g also dependent on the state X and control U. The nonlinear model in represented by Eq. (10) and Eq. (11) and the state and control vector are defined in sequence by the Eq. (12) and Eq. (13).

$$\dot{X} = f(X, U) \tag{10}$$

$$Y = g(X, U) \tag{11}$$

$$X = \begin{bmatrix} V & \alpha & \theta & q & H & \beta & \phi & p & r & \psi & X_0 & Y_0 & E & Q \end{bmatrix}^T \tag{12}$$

Where V is ground speed, α angle of attack, θ pitch attitude, q pitch angular velocity, H altitude, β sideslip angle, ϕ roll attitude, p roll angular velocity, r yaw angular velocity, ψ yaw attitude, X_0 and Y_0 coordinates in the earth system and Q the amount of current drained from the battery.

$$U = \begin{bmatrix} \delta_e & \pi & \delta_a & \delta_r \end{bmatrix}^T \tag{13}$$

The mechanical model applied is the one presented by Stevens, Lewis and Johnson (2016) for a rigid body with six degrees of freedom; the author defines the set of equations bellow to estimate the derivatives of each state variables formerly presented.

Force equations:

$$\dot{u} = rv - qw - g\sin(\theta) + F_X / m \tag{14}$$

$$\dot{v} = -ru + pw + g\sin(\phi)\cos(\theta) + F_Y / m \tag{15}$$

$$\dot{w} = qu - pv + g\cos(\phi)\cos(\theta) + F_Z / m \tag{16}$$

Kinematic equations:

$$\dot{\phi} = p + \tan(\theta)\left(q\sin(\phi) + r\cos(\phi)\right) \tag{17}$$

$$\dot{\theta} = q\cos(\phi) - r\sin(\phi) \tag{18}$$

$$\dot{\psi} = \left(q\sin(\phi) + r\cos(\phi)\right)/\cos(\theta) \tag{19}$$

Moment equations:

$$\Gamma\dot{p} = J_{XZ}\left(J_X - J_Y + J_Z\right)pq - \left(J_Z\left(J_Z - J_Y\right) + {J_{XZ}}^2\right)qr + J_Z\ell + J_{XZ}n \tag{20}$$

$$J_Y\dot{q} = \left(J_Z - J_X\right)pr - J_{XZ}\left(p^2 - r^2\right) + m \tag{21}$$

$$\Gamma\dot{r} = \left(\left(J_X - J_Y\right)J_X + {J_{XZ}}^2\right)pq - J_{XZ}\left(J_X - J_Y + J_Z\right)qr + J_{XZ}\ell + J_X n \tag{22}$$

$$\Gamma = J_X J_Z - {J_{XZ}}^2 \tag{23}$$

Where J_X, J_Y, J_Z and J_{XZ} are the body moments of inertia.

Navigations equations (sine and cosine represented by *s* and *c*):

$$\dot{X}_0 = uc\theta c\psi + v\left(-c\phi s\psi + s\phi s\theta c\psi\right) + w\left(s\phi s\psi + c\phi c\theta c\psi\right) \tag{24}$$

$$\dot{Y}_0 = uc\theta s\psi + v\left(c\phi c\psi + s\phi s\theta s\psi\right) + w\left(-s\phi c\psi + c\phi s\theta s\psi\right) \tag{25}$$

$$\dot{H} = us\theta - vs\phi c\theta - wc\phi c\theta \tag{26}$$

Finally, the battery state of charge derivative is the electrical current:

$$\dot{Q} = I \tag{27}$$

3. CONTROL SYSTEMS

The design of the control systems was executed accordingly as proposed by Stevens, Lewis and Johnson (2016) for optimal control with multiple inputs and multiples outputs (MIMO), this is done by trimming the airplane in the desired flight condition and then linearizing the model to allow control techniques to be applied. The optimal gains for the system are found by minimizing a performance index described by the authors, this was done aided by optimization solvers available in MATLAB environment. The simulation block diagram is shown in Fig. 5, where a generic autopilot (AP) can be seen, having in the inner loop a stability augmentation system (SAS) and in the outer loop a compensator.

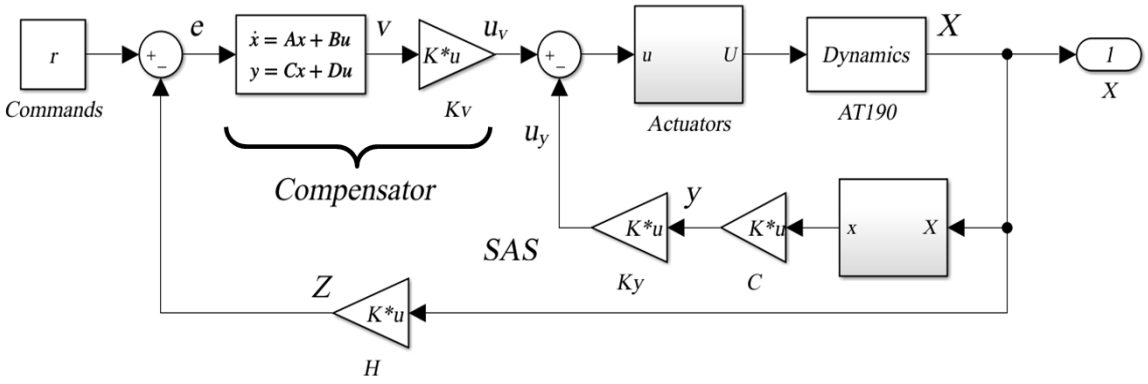

Figure 5. Simulation block diagram.
Source: Author.

For the present work all the control systems bellow were implemented, being designed using whether PI, PD or PID compensators:

- Pitch-attitude hold AP: tracks θ and regulates q;
- Altitude hold AP: tracks altitude H and integrates the pitch-attitude hold AP as a SAS;
- Speed hold AP: tracks speed V and integrates the pitch-attitude hold AP as a SAS;
- Yaw damper SAS: regulates the angular velocities p and r;
- Roll angle hold AP: tracks roll attitude ϕ and regulates p
- Turn coordination AP: tracks the sideslip angle β.

4. RESULTS

Steady state flight was simulated until the battery voltage reached its lower limit, this way was possible to estimate characteristics like range, endurance, absolute ceiling, minimum and maximum flight velocity and others.

The simulations were done at sea level conditions, matching the International Standard Atmosphere (ISA), as initial altitude for climb simulations and as stop criteria for descents. For the last case the initial altitude was 300 meters, a number that correspond to the flight altitude usually employed in mission.

4.1. Analysis of the Control systems

First, a quick simulation was carried to ensure that the control system is capable of maintaining the airplane. in the desired attitude. In order to accomplish this, a wind shear model was inserted in the simulation and the aircraft was forced to pass through the wind. The wind modeled has a maximum vertical speed component (V_{WZ}) of 5 m/s (downward), a horizontal component (V_{WH}) up to 5 m/s as well and the wind shear diameter is 120 m. The wind speed distribution along the radius (r) is as follows:

$$V_{WH} = 5 \cdot \sin(\pi \cdot r/60) \quad \text{if} \quad -60 \le r \le 60 \tag{28}$$

$$V_{WZ} = 5 \cdot \cos(\pi/2 \cdot r/60) \quad \text{if} \quad -60 \le r \le 60 \tag{29}$$

$$V_{WH} = 0 \quad \text{if} \quad r < -60 \quad \text{or} \quad r > 60 \tag{30}$$

$$V_{WZ} = 0 \quad \text{if} \quad r < -60 \quad \text{or} \quad r > 60 \tag{31}$$

As a result, Fig. 6 shows that even subjected to wind disturbances the control system was able to maintain the aircraft in the initial condition with subtle differences in attitude.

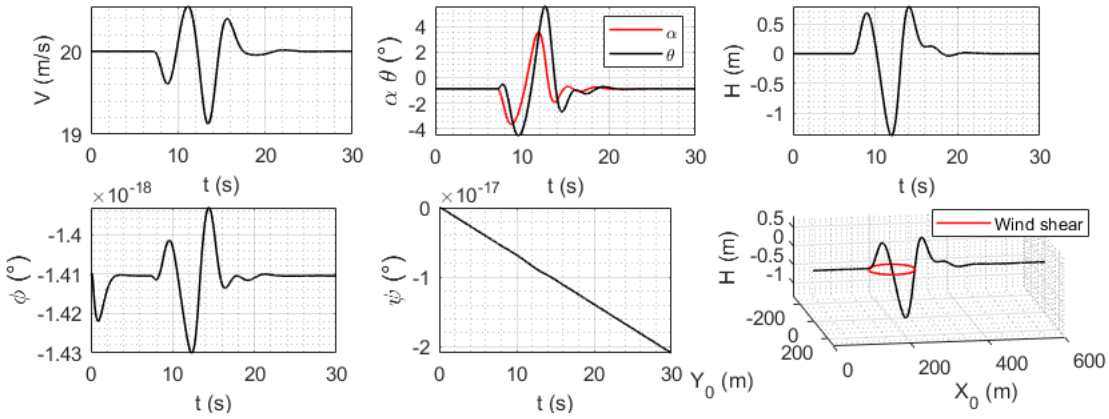

Figure 6. Wind shear response – state variables.
Source: Author.

Furthermore, in the image bellow is possible to see the active and smooth work of the actuators during the disturbances applied.

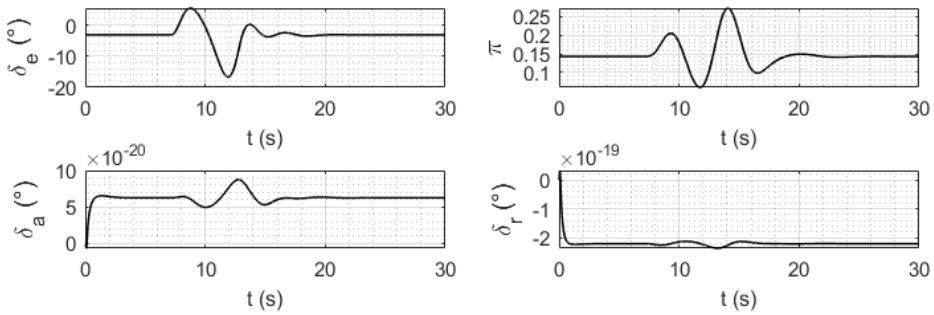

Figure 7. Wind shear response – control variables.
Source: Author.

4.2. Level Fligth

Figure 8 shows the curves of maximum range and endurance as a function of velocity, three conditions are highlighted: maximum speed, maximum range and endurance. Detailed information about the performance in constant altitude and straight path are shown below in Table 2.

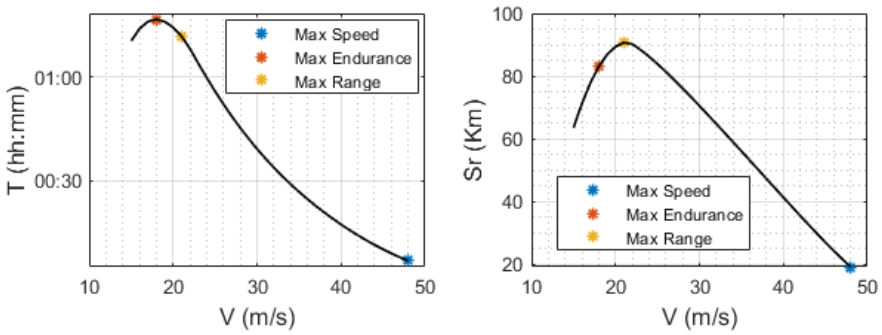

Figure 8. Cruise flight range and endurance versus speed.
Source: Author.

Table 2. Cruise flight performance.

Cruise flight	V (m/s)	T (min)	S_R (km)
Maximum speed V_{max}	48.0	6.6	19.2
Maximum endurance T	18.0	76.8	83.0
Maximum range S_R	21.0	71.9	90.6

Source: Author

Differently from cruise flight, in turns the points of interest are minimum radius R_{min}, maximum endurance T_{max} and maximum angular range ψ_R. These values are organized in the table below, note that the velocity in which minimum turn radius is achieved is the same for maximum turning rate.

Table 3. Turning flight performance.

Turning flight	V (m/s)	$\dot{\psi}$ (°/s)	R (m)	T_{max} (min)	ψ_R (rev.*)
Minimum radius R_{min}	17.0	33.05	29.47	43.4	239.1
Maximum endurance T	22.0	25.54	49.35	52.7	222.7
Maximum range ψ_R	18.0	31.22	33.04	46.6	242.6

* rev: means revolutions

Source: Author.

In addition to the results presented, the flight envelopes were drawn. For both rectilinear and turning paths, the main information obtained are exposed bellow in Table 4 and the envelopes are seen in Fig. 9.

Table 4. Maximum range and endurance for flight altitude.

Rectilinear flight	V (m/s)	H (m)	T_{max} (min)	S_{rmax} (km)
Absolute ceiling	41.89	13200	5.9	14.8
Operational ceiling	17.41 – 48.78	3000	54.4	75.8
Turning flight	V (m/s)	H (m)	T_{max} (min)	Ψ_{rmax} (rev.*)
Absolute ceiling	42.00	10922	2.4	14.1
Operational ceiling	19.75 – 48.83	3000	36.6	141.0

* rev. represents revolutions.

Source: Author.

It can be seen in the figures a dashed line marking the operational ceiling on 3000 m, this was defined as a reasonable limit, since the airplane itself does not have means to reach such altitude.

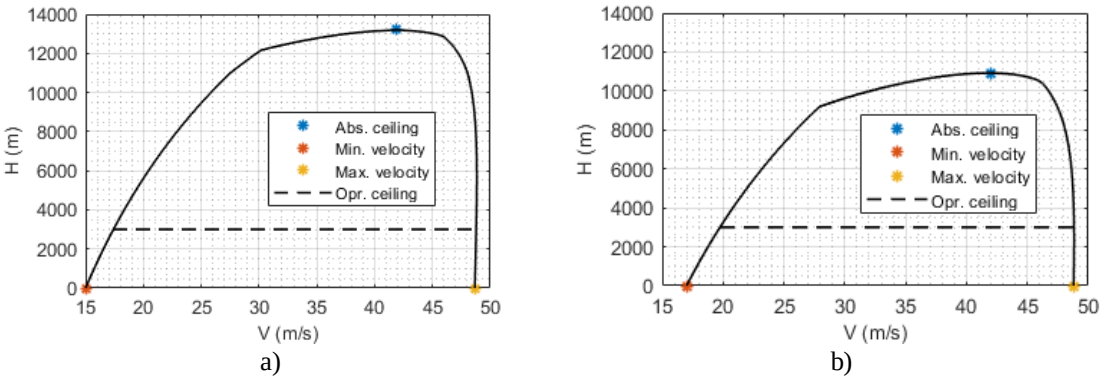

Figure 9. Flight envelopes. a) Rectilinear flight. b) Turning flight.
Source: Author.

4.3. Climb and Gliding Fligth

As a result of climb and glide simulations the speed polars were drawn, Fig. 10. Additional information is provided in Table 5

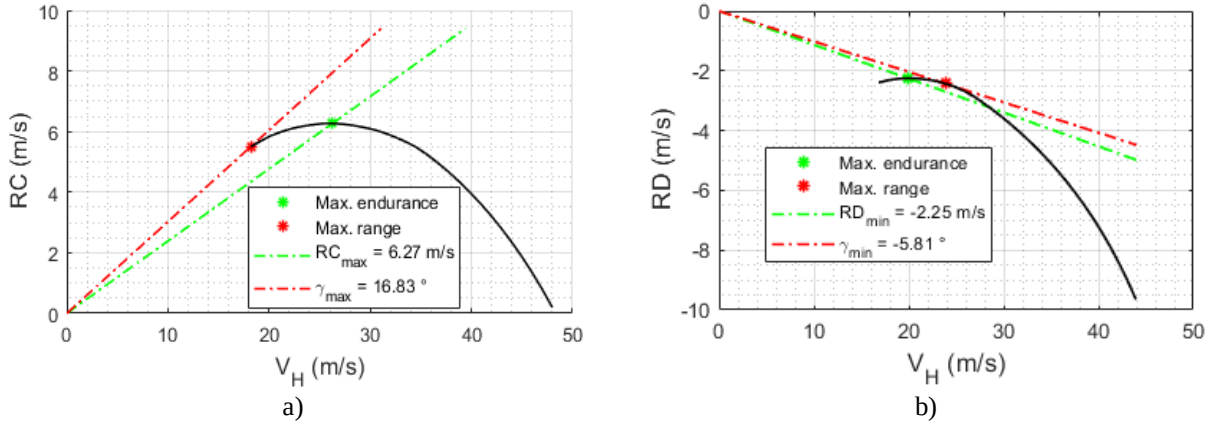

Figure 10. Speed polars. a) Climb. b) Gliding.
Source: Author.

Table 5. Climb and gliding performance.

Climb flight		*V* (m/s)
Maximum rate of climb *RC*	6.27 m/s	27.0
Maximum angle of climb γ	16.8 °	19.0
Maximum vertical range H_r	1848.1 m	27
Gliding flight		*V* (m/s)
Minimum rate of descent *RD*	2.25 m/s	20.0
Minimum angle of descent γ	5.81 °	24.0

Source: Author

4.4. Operational radius

At last, a simulation of a simplified mission was carried with the purpose of estimating the system operational radius. The mission simulated consists of a climb, starting from sea level until 300 meters at 18 m/s and flight angle of 15 degrees in a 150 m radius loiter. Then level straight flight at 20 m/s until the battery voltage reaches the lower limit of 14.2 V. Finally, the airplane descends at 17 m/s with a flight angle of -5 degrees in a 150 m radius loiter until it reaches sea level altitude.

The simulation state and control variables are shown in Fig. 11 and 12, respectively, and little disturbances can be seen during transitions between climb, cruise and gliding flight.

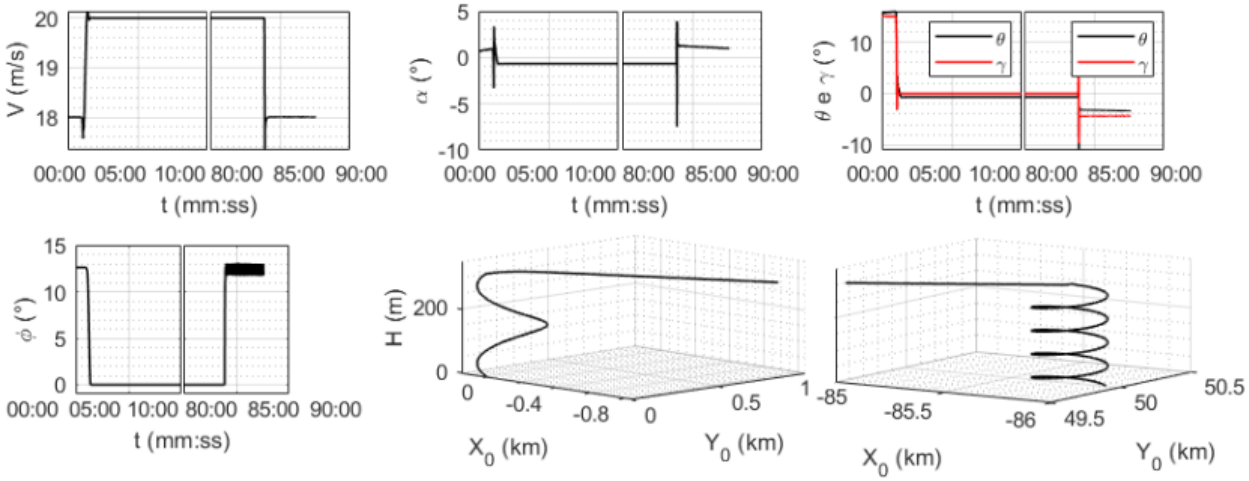

Figure 11. Simulation of a simplified mission – state variables.
Source: Author.

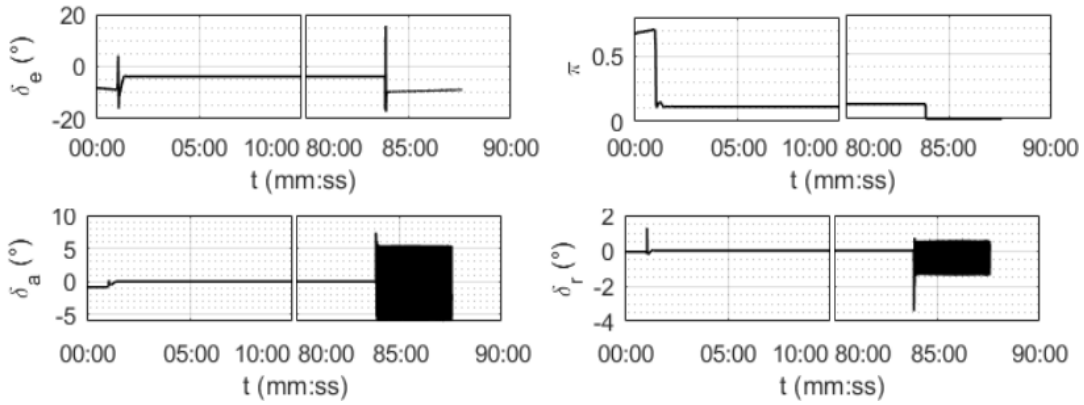

Figure 12. Simulation of a simplified mission – control variables.
Source: Author.

Figure13 shows that even though the cruise flight is aborted after the battery voltage reaches 14.2 V and the airplane still must descend back to takeoff altitude, the final voltage is above 14.2 V. This is an interesting fact that occurs due to internal resistance in battery circuit.

As a result, it was found a nominal endurance of 87.6 minutes and range of 100.5 km. Consequently, the operational radius is 50.25 km.

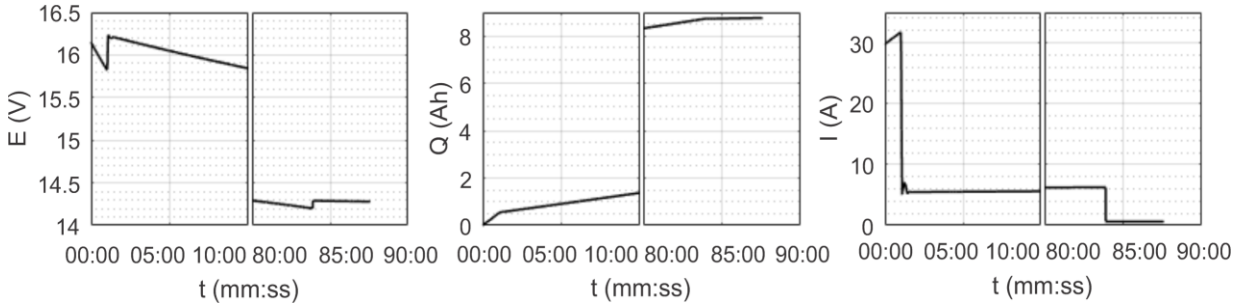

Figure 13. Simulation of a simplified mission – battery state.
Source: Author.

5. REFERENCES

COOK, M. V. “Flight Dynamics Principles**:** A Linear System Approach to Aircraft Stability and Control”. 2nd ed. Burlington, MA: Elsevier, 2007.

MAOQUAN, Z.; HAIXIN, C. “Modeling and validation of propulsive system for small battery powered electric aircraft”. *EUROPEAN CONFERENCE FOR AERONAUTICS AND SPACE SCIENCES. [S.l.: s.n.], 2017*. Available at < https://www.eucass.eu/doi/EUCASS2017-701.pdf >

ROSKAM, J. “Airplane design: Part V: Preliminary Calculation of Aerodynamics, Thrust and Power Characteristics”. First printing. Ottawa, KA, 1987.

ROSKAM, J. “Airplane Flight Dynamics and Automatic Flight Controls”. Third printing. Lawrence, KA: DARcorporation, 2001.

ROSKAM, J. “Methods for Estimating Stability and Control Derivatives of Conventional Subsonics Airplanes”. Second printing. Lawrence, KA, 1973.

STEVENS; B.; LEWIS, F. L.; JOHNSON, E. N. Aircraft Control and Simulation: Dynamics, Control Design and Autonomous Systems. 3rd ed. Hoboken, NJ: John Wiley & Sons, 2016.

6. RESPONSIBILITY NOTICE

The authors are the only responsible for the printed material included in this paper.